# 25

# Frequency Mixing Effects in Graphene

Sergey Mikhailov
*University of Augsburg*
*Germany*

## 1. Introduction

Graphene is a new nanomaterial which has been discovered a few years ago, Novoselov et al. (2004); Novoselov et al. (2005); Zhang et al. (2005) and has demonstrated unique mechanical, electrical, thermal and optical properties, see review articles Katsnelson (2007); Castro Neto et al. (2009); Geim (2009). This is a one-atom-thick layer of carbon atoms arranged in a highly symmetric two-dimensional honey-comb lattice, Figure 1. Graphene exhibits many interesting fundamental physical properties such as the minimal electrical conductivity Novoselov et al. (2005); Zhang et al. (2005); Katsnelson (2006); Nomura & MacDonald (2007); Tan et al. (2007), unconventional quantum Hall effect Novoselov et al. (2005); Zhang et al. (2005) observable up to room temperatures Novoselov et al. (2007), Klein tunneling Stander et al. (2009); Young & Kim (2009), optical conductivity determined only by the fine structure constant Ando et al. (2002); Kuzmenko et al. (2008); Nair et al. (2008) and many other. Graphene promises many electronic applications like terahertz transistors, photodetectors, transparent electrodes for displays, gas and strain sensors and so on, Geim (2009).

Microscopically, the most distinguished feature of graphene is that, in contrast to other (semiconductor) materials with two-dimensional electron gases, electrons and holes in graphene have not a parabolic, but a linear energy spectrum near the Fermi level Wallace (1947); McClure (1956); Slonczewski & Weiss (1958). The Brillouin zone of graphene electrons has a hexagonal shape, Figure 2, and near the corners $\mathbf{K}_j$, $j = 1, \ldots 6$, the electron and hole energy bands $E_{l\mathbf{p}}$ touch each other; here $\mathbf{p}$ is the quasi-momentum of an electron and $l$ is the band index ($l = 1$ for holes and $l = 2$ for electrons). The spectrum $E_{l\mathbf{p}}$ near these, so called Dirac points is linear,

$$E_{l\mathbf{p}} = (-1)^l V|\mathbf{p} - \hbar\mathbf{K}_j| = (-1)^l V|\tilde{\mathbf{p}}| = (-1)^l \hbar V|\mathbf{k} - \mathbf{K}_j|, \tag{1}$$

where $\mathbf{k}$ is the quasi-wavevector, $\tilde{\mathbf{p}} = \mathbf{p} - \hbar\mathbf{K}_j$ and $V$ is the Fermi velocity. In graphene $V \approx 10^8$ cm/s, so that electrons and holes behave like massless "relativistic" particles with the effective "velocity of light" $V \approx c/300$, where $c$ is the real velocity of light. In the intrinsic graphene the chemical potential $\mu$ (or the Fermi energy $E_F$) goes through Dirac points, $\mu = 0$. If graphene is doped or if a dc (gate) voltage is applied between the graphene layer and a semiconductor substrate (in a typical experiment the graphene sheet lies on a substrate, e.g. on Si-$SiO_2$) the chemical potential can be shifted to the upper or lower energy band, so that the electron or hole density $n_s$ can be varied from zero up to $\approx 10^{13}$ cm$^{-2}$. It is the unusual "relativistic" energy dispersion of graphene electrons (1) that leads to the unique physical properties of graphene.

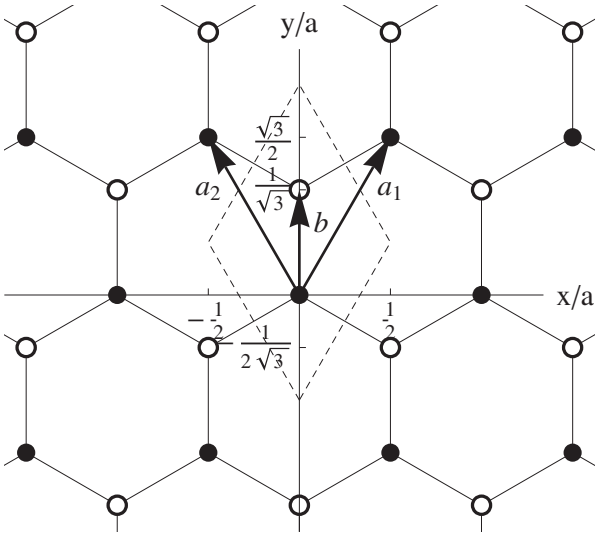


Fig. 1. The honey-comb lattice of graphene. All points of the sublattice A (black circles) are given by $n_1\mathbf{a}_1 + n_2\mathbf{a}_2$, of the sublattice B (open circles) by $n_1\mathbf{a}_1 + n_2\mathbf{a}_2 + \mathbf{b}$. Dashed lines show the boundaries of the elementary cell. $a$ is the lattice constant.

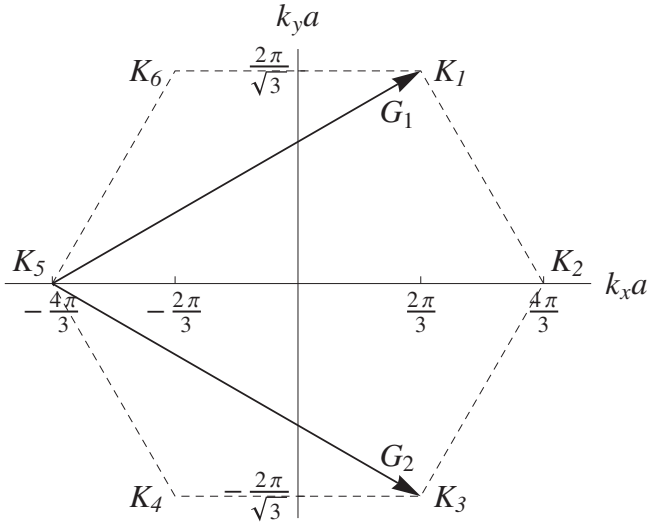


Fig. 2. The Brillouin zone of graphene. The basis vectors of the reciprocal lattice are $\mathbf{G}_1$ and $\mathbf{G}_2$. The vectors $\mathbf{K}_j$, $j = 1, \ldots, 6$, correspond to the corners of the Brillouin zone (the Dirac points). Here $\mathbf{K}_1 = -\mathbf{K}_4 = 2\pi a^{-1}(1/3, 1/\sqrt{3})$, $\mathbf{K}_2 = -\mathbf{K}_5 = 2\pi a^{-1}(2/3, 0)$, $\mathbf{K}_3 = -\mathbf{K}_6 = 2\pi a^{-1}(1/3, -1/\sqrt{3})$.

In 2007 it was predicted Mikhailov (2007) that the *linear* spectrum of graphene electrons (1) should lead to a *strongly nonlinear* electromagnetic response of this material. The physical

origin of this effect is very simple. As seen from (1) the graphene electrons cannot stop and can move only with the velocity $V$. If such a particle is placed in the uniform oscillating electric field $\mathbf{E}(t) = \mathbf{E}_0 \cos \omega t$, its momentum will oscillate as $\mathbf{p}(t) \propto \sin \omega t$. The velocity of such particles $\mathbf{v} = \partial E_{l\mathbf{p}} / \partial \mathbf{p} = V \tilde{\mathbf{p}} / |\tilde{\mathbf{p}}|$ will then take the value of $+V$ or $-V$ dependent on the sign of the momentum $\tilde{\mathbf{p}}$, i.e. $\mathbf{v}(t) \propto \mathrm{sgn}(\sin \omega t)$. The electric current $\mathbf{j}(t)$ induced by the external field is determined by the velocity, therefore one will have [1]

$$\mathbf{j}(t) \propto \mathrm{sgn}(\sin \omega t) = \frac{4}{\pi} \left( \sin \omega t + \frac{1}{3} \sin 3\omega t + \frac{1}{5} \sin 5\omega t + \dots \right). \tag{2}$$

The induced current thus contains higher frequency harmonics $n\omega$, $n = 3, 5, \dots$ and hence a single graphene sheet should radiate electromagnetic waves not only at the frequency $\omega$ but also at $n\omega$ with $n = 3, 5, 7, \dots$ Mikhailov (2007; 2008); Mikhailov & Ziegler (2008). Graphene could thus serve as a simple and inexpensive frequency multiplier Mikhailov (2007; 2009). The nonlinear electromagnetic response of graphene has been also discussed by López-Rodríguez & Naumis (2008).

Apart from the frequency multiplication effect all other known nonlinear electromagnetic phenomena should be also observable in this material. For example, irradiation of the graphene layer by two electromagnetic waves $\mathbf{E}_1(t)$ and $\mathbf{E}_2(t)$ with the frequencies $\omega_1$ and $\omega_2$ should lead to the emission of radiation at the mixed frequencies $n_1\omega_1 + n_2\omega_2$ with integer numbers $n_1$ and $n_2$. Since the graphene lattice (Figure 1) has a central symmetry, the even order effects are forbidden in the infinite and uniform graphene layer, so that $n_1 + n_2$ must be an odd integer. In the third order in the external field amplitudes $\mathbf{E}_1$ and $\mathbf{E}_2$, apart from the frequencies $\omega_1, \omega_2, 3\omega_1$ and $3\omega_2$, the radiation at the mixed frequencies $\omega_1 \pm 2\omega_2$ and $2\omega_1 \pm \omega_2$ should be observed. In a recent experiment Hendry et al. (2010) the coherent emission from graphene at the frequency $2\omega_1 - \omega_2$ has indeed been discovered in the near-infrared and visible frequency range.

In this Chapter we develop a theory of the frequency mixing effect in graphene. We begin with a discussion of the electronic spectrum and the wave functions of graphene obtained in the tight-binding approximation (Section 2) and continue by a brief overview of the linear response theory of graphene in Section 3. Then we study the frequency mixing effects in graphene within the framework of the quasi-classical approach which works on low (microwave, terahertz) frequencies (Section 4). In Section 5 we introduce a quantum theory of the nonlinear electromagnetic response of graphene to high (infrared, optical) frequencies. A summary of results and the prospects for future research are discussed in Section 6.

## 2. Energy spectrum and wave functions of graphene

We calculate the spectrum and the wave functions of graphene electrons within the framework of the tight-binding approximation Wallace (1947); Reich et al. (2002) assuming that both the overlap and the transfer integrals are nonzero only for the nearest-neighbor atoms. The lattice of graphene, Figure 1, consists of two triangular sublattices A and B. For the basic vectors of the A lattice we choose the vectors $\mathbf{a}_1 = a(1/2, \sqrt{3}/2)$ and $\mathbf{a}_2 = a(-1/2, \sqrt{3}/2)$, where $a$ is the lattice constant ($a \approx 2.46$ Å in graphene). The vector $\mathbf{b}$ connecting the sublattices is

[1] In conventional electron systems with the parabolic spectrum of charge carriers $E_{\mathbf{p}} = p^2/2m^\star$ the velocity $\mathbf{v} = \partial E_{\mathbf{p}} / \partial \mathbf{p} = \mathbf{p}/m^\star$ is proportional to the momentum, therefore $\mathbf{j} \propto \mathbf{v} \propto \sin \omega t$ and the higher frequency harmonics are not generated.

$\mathbf{b} = a(0, 1/\sqrt{3})$. The two-dimensional single-particle Hamiltonian $\hat{H}_0$ of graphene can then be written as

$$\hat{H}_0 = \frac{\hat{\mathbf{p}}^2}{2m} + \sum_{\mathbf{a}}[U_a(\mathbf{r}-\mathbf{a}) + U_a(\mathbf{r}-\mathbf{a}-\mathbf{b})], \tag{3}$$

where $\hat{\mathbf{p}} = -i\hbar(\partial_x, \partial_y)$ is the two-dimensional momentum operator, $m$ is the free electron mass and $U_a$ is the atomic potential. Following the standard procedure of the tight binding approximation we get the energy $E_{l\mathbf{k}}$ and the wave functions $|l\mathbf{k}\rangle$ of graphene electrons as

$$E_{l\mathbf{k}} = (-1)^l t|\mathcal{S}_{\mathbf{k}}|, \tag{4}$$

$$|l\mathbf{k}\rangle \equiv \Psi_{l\mathbf{k}}(\mathbf{r}) = \frac{1}{\sqrt{S}} e^{i\mathbf{k}\cdot\mathbf{r}} u_{l\mathbf{k}}(\mathbf{r}), \tag{5}$$

$$u_{l\mathbf{k}}(\mathbf{r}) = \sqrt{\frac{A}{2}} \sum_{\mathbf{a}} e^{-i\mathbf{k}\cdot(\mathbf{r}-\mathbf{a})} \left[(-1)^l \zeta_{\mathbf{k}} \psi_a(\mathbf{r}-\mathbf{a}) + \psi_a(\mathbf{r}-\mathbf{a}-\mathbf{b})\right], \tag{6}$$

where $l = 1, 2$, $\mathbf{k} = (k_x, k_y)$ is the quasi-wavevector, $t$ is the transfer integral (in graphene $t \approx 3$ eV), $S$ and $A$ are the areas of the sample and of the elementary cell, respectively, and $\psi_a$ is the atomic wave function. The functions $\mathcal{S}_{\mathbf{k}}$ and $\zeta_{\mathbf{k}}$ in (4) and (6) are defined as

$$\mathcal{S}_{\mathbf{k}} = 1 + e^{i\mathbf{k}\cdot\mathbf{a}_1} + e^{i\mathbf{k}\cdot\mathbf{a}_2} = 1 + 2\cos(k_x a/2) e^{i\sqrt{3}k_y a/2}, \tag{7}$$

$$\zeta_{\mathbf{k}} = \mathcal{S}_{\mathbf{k}}/|\mathcal{S}_{\mathbf{k}}|. \tag{8}$$

They are periodic in the $\mathbf{k}$-space and satisfy the equalities

$$\mathcal{S}_{-\mathbf{k}} = \mathcal{S}^\star_{\mathbf{k}};\ \ \mathcal{S}_{\mathbf{k}+\mathbf{G}} = \mathcal{S}_{\mathbf{k}};\ \ \zeta_{-\mathbf{k}} = \zeta^\star_{\mathbf{k}};\ \ \zeta_{\mathbf{k}+\mathbf{G}} = \zeta_{\mathbf{k}}; \tag{9}$$

where $\mathbf{G}$ are the 2D reciprocal lattice vectors. Similar relations are valid for the energies $E_{l\mathbf{k}}$ and the wave functions $\Psi_{l\mathbf{k}}(\mathbf{r})$,

$$E_{l,-\mathbf{k}} = E_{l\mathbf{k}};\ \ \Psi_{l,-\mathbf{k}}(\mathbf{r}) = \Psi^\star_{l\mathbf{k}}(\mathbf{r});\ \ E_{l,\mathbf{k}+\mathbf{G}} = E_{l\mathbf{k}};\ \ \Psi_{l,\mathbf{k}+\mathbf{G}}(\mathbf{r}) = \Psi_{l\mathbf{k}}(\mathbf{r}). \tag{10}$$

The basic reciprocal lattice vectors $\mathbf{G}_1$ and $\mathbf{G}_2$ can be chosen as $\mathbf{G}_1 = (2\pi/a)(1, 1/\sqrt{3})$, $\mathbf{G}_2 = (2\pi/a)(1, -1/\sqrt{3})$, see Figure 2.

The energy dispersion (4) is shown in Figure 3. At the corners of the Brillouin zone, in the Dirac points $\mathbf{k} = \mathbf{K}_j$, the function $\mathcal{S}_{\mathbf{k}}$ vanishes and at $|\mathbf{k} - \mathbf{K}_j|a = |\delta\mathbf{k}_j|a \ll 1$ one has

$$\mathcal{S}_{\mathbf{k}} \approx -\frac{\sqrt{3}a}{2}\left[(-1)^j \delta k^j_x + i\delta k^j_y\right], \tag{11}$$

$$\zeta_{\mathbf{k}} = -\frac{(-1)^j \delta k^j_x + i\delta k^j_y}{\sqrt{(\delta k^j_x)^2 + (\delta k^j_y)^2}}. \tag{12}$$

The energy (4) then assumes the form (1) with the velocity $V = \sqrt{3}ta/2\hbar \approx 10^8$ cm/s.

Using the wave functions (5)–(6) one can calculate the matrix elements of different physical quantities. For example, for the function $e^{i\mathbf{q}\cdot\mathbf{r}}$ we get

$$\langle l'\mathbf{k}'|e^{i\mathbf{q}\cdot\mathbf{r}}|l\mathbf{k}\rangle = \frac{1}{2}\delta_{\mathbf{k}',\mathbf{k}+\mathbf{q}}\left[1 + (-1)^{l'+l}\zeta^\star_{\mathbf{k}+\mathbf{q}}\zeta_{\mathbf{k}}\right]. \tag{13}$$

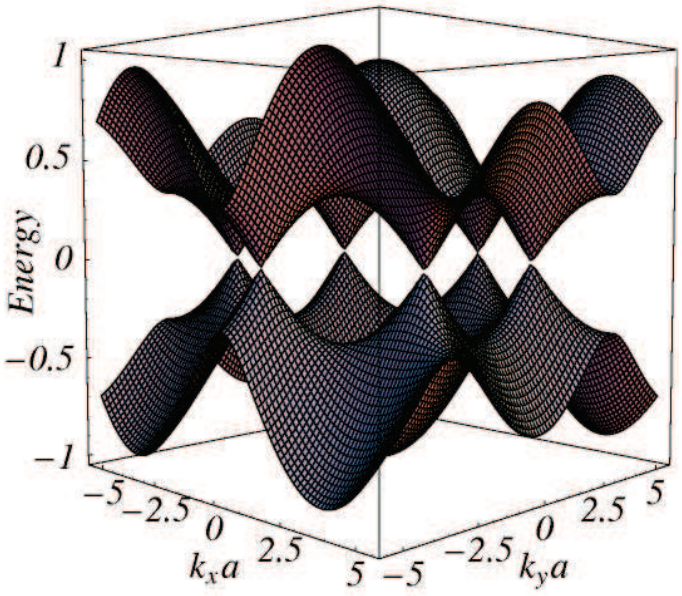


Fig. 3. The bandstructure of graphene electrons $E_{l\mathbf{k}}$ calculated in the tight-binding approximation, Eq. (4).

In the limit $\mathbf{q} \to \mathbf{0}$ we obtain from here the matrix elements of the coordinate

$$\langle l'\mathbf{k}|\hat{x}_\alpha|l\mathbf{k}\rangle = \frac{i}{2}(-1)^{l'+l}\zeta^\star_{\mathbf{k}}\frac{\partial\zeta_{\mathbf{k}}}{\partial k_\alpha} \tag{14}$$

and of the velocity operator $\hat{\mathbf{v}} = \hat{\mathbf{p}}/m$,

$$\langle l\mathbf{k}|\hat{v}_\alpha|l\mathbf{k}\rangle = \frac{1}{\hbar}\frac{\partial E_{l\mathbf{k}}}{\partial k_\alpha}, \quad \langle l\mathbf{k}|\hat{v}_\alpha|\bar{l}\mathbf{k}\rangle = \frac{E_{l\mathbf{k}} - E_{\bar{l}\mathbf{k}}}{2\hbar}\zeta^\star_{\mathbf{k}}\frac{\partial\zeta_{\mathbf{k}}}{\partial k_\alpha}. \tag{15}$$

Here $\bar{l}$ means *not* $l$, i.e. $\bar{l} = 2$ if $l = 1$ and $\bar{l} = 1$ if $l = 2$.

## 3. Linear response

Before presenting our new results on the nonlinear frequency mixing effects we will briefly overview the linear response theory of graphene. We will calculate the linear response dynamic conductivity of graphene $\sigma^{(1)}(\omega) \equiv \sigma(\omega)$ which has been studied theoretically in Refs. Gusynin & Sharapov (2006); Gusynin et al. (2006); Nilsson et al. (2006); Abergel & Fal'ko (2007); Falkovsky & Pershoguba (2007); Falkovsky & Varlamov (2007); Mikhailov & Ziegler (2007); Peres et al. (2008); Stauber, Peres & Castro Neto (2008) and experimentally in Refs. Dawlaty et al. (2008); Li et al. (2008); Mak et al. (2008); Stauber, Peres & Geim (2008).

### 3.1 Quantum kinetic equation

The system response is described by the quantum kinetic (Liouville) equation

$$i\hbar\frac{\partial\hat{\rho}}{\partial t} = [\hat{H}, \hat{\rho}] \tag{16}$$

for the density matrix $\hat{\rho}$, where

$$\hat{H} = \hat{H}_0 + \hat{H}_1 = \hat{H}_0 - e\phi(\mathbf{r}, t), \tag{17}$$

is the Hamiltonian of graphene in the presence of the external electric field $\mathbf{E}(\mathbf{r}, t) = -\nabla\phi(\mathbf{r}, t)$ and $e > 0$ is the electron charge. We will be interested in the response to the uniform electric field but at this step will describe the electric field by the potential

$$\phi(\mathbf{r}, t) = \phi_{\mathbf{q}\omega} e^{i\mathbf{q}\cdot\mathbf{r} - i\omega t + \gamma t}, \;\; \gamma \to +0, \tag{18}$$

and will take the limit $\mathbf{q} \to \mathbf{0}$ later on. The unperturbed Hamiltonian $\hat{H}_0$ is given by Eq. (3). It has the eigenenergies and eigenfunctions,

$$\hat{H}_0 |l\mathbf{k}\sigma\rangle = E_{l\mathbf{k}} |l\mathbf{k}\sigma\rangle, \tag{19}$$

given by equations (4) and (5), respectively; we have also introduced the spin index $\sigma$ here. Expanding the density matrix up to the first order in the electric field,

$$\hat{\rho} = \hat{\rho}_0 + \hat{\rho}_1, \tag{20}$$

where $\hat{\rho}_0$ satisfies the equation

$$\hat{\rho}_0 |l\mathbf{k}\sigma\rangle = f_0(E_{l\mathbf{k}}) |l\mathbf{k}\sigma\rangle, \tag{21}$$

and $f_0$ is the Fermi function, we get

$$\langle l'\mathbf{k}'\sigma' | \hat{\rho}_1 | l\mathbf{k}\sigma\rangle = \frac{f_0(E_{l'\mathbf{k}'}) - f_0(E_{l\mathbf{k}})}{E_{l'\mathbf{k}'} - E_{l\mathbf{k}} - \hbar(\omega + i0)} \langle l'\mathbf{k}'\sigma' | \hat{H}_1 | l\mathbf{k}\sigma\rangle, \tag{22}$$

$$\langle l'\mathbf{k}'\sigma' | \hat{H}_1 | l\mathbf{k}\sigma\rangle = -e\phi_{\mathbf{q}\omega}\delta_{\sigma\sigma'} \langle l'\mathbf{k}' | e^{i\mathbf{q}\cdot\mathbf{r}} | l\mathbf{k}\rangle. \tag{23}$$

Calculating the first order current $\mathbf{j}(\mathbf{r}, z, t) = \mathbf{j}_{\mathbf{q}\omega} e^{i\mathbf{q}\cdot\mathbf{r} - i\omega t + \gamma t}\delta(z)$ we obtain

$$\begin{aligned} \mathbf{j}_{\mathbf{q}\omega} &= -\frac{e}{2S}\mathrm{Sp}\left(\hat{\rho}_1 [\hat{\mathbf{v}}, e^{-i\mathbf{q}\cdot\mathbf{r}}]_+\right) \\ &= \frac{e^2 g_s}{2S}\phi_{\mathbf{q}\omega} \sum_{\mathbf{k}\mathbf{k}' ll'} \langle l\mathbf{k} | [\hat{\mathbf{v}}, e^{-i\mathbf{q}\cdot\mathbf{r}}]_+ | l'\mathbf{k}'\rangle \frac{f_0(E_{l'\mathbf{k}'}) - f_0(E_{l\mathbf{k}})}{E_{l'\mathbf{k}'} - E_{l\mathbf{k}} - \hbar(\omega + i\gamma)} \langle l'\mathbf{k}' | e^{i\mathbf{q}\cdot\mathbf{r}} | l\mathbf{k}\rangle, \end{aligned} \tag{24}$$

where $\mathbf{j} = (j_x, j_y)$ and $[\ldots]_+$ denotes the anti-commutator. Taking the limit $\mathbf{q} \to \mathbf{0}$ gives the frequency dependent conductivity $\sigma_{\alpha\beta}(\omega)$ which describes the linear response of graphene to a uniform external electric field. The conductivity $\sigma_{\alpha\beta}(\omega)$ consists of two contributions, the intra-band ($l = l'$) and the inter-band ($l \neq l'$) conductivities.

### 3.2 Intra-band conductivity

The intra-band conductivity reads

$$\sigma_{\alpha\beta}^{intra}(\omega) = \frac{-ie^2 g_s}{\hbar^2(\omega + i\gamma)S} \sum_{l\mathbf{k}} \frac{\partial E_{l\mathbf{k}}}{\partial k_\alpha} \frac{\partial f_0(E_{l\mathbf{k}})}{\partial E} \frac{\partial E_{l\mathbf{k}}}{\partial k_\beta}, \tag{25}$$

where $g_s = 2$ is the spin degeneracy and the summation over $\mathbf{k}$ is performed over the whole Brillouin zone. If the chemical potential $\mu$ lies within $\sim 1$ eV from the Dirac points (which is typically the case in the experiments) and if the photon energy $\hbar\omega$ does not exceed $1 - 2$ eV

the main contribution to the integrals is given by the vicinity of Dirac points and one can use the linear (Dirac) approximation (11), (1). Then one gets $\sigma^{intra}_{\alpha\beta}(\omega) = \sigma^{intra}(\omega)\delta_{\alpha\beta}$ and

$$\sigma^{intra}(\omega) = \frac{ie^2 g_s g_v T}{2\pi\hbar^2(\omega + i\gamma)} \ln\left[2\cosh\left(\frac{\mu}{2T}\right)\right], \tag{26}$$

where $T$ is the temperature and $g_v = 2$ is the valley degeneracy factor. At low temperatures $T \ll |\mu|$ the formula (26) gives

$$\sigma^{intra}(\omega) = \frac{e^2 g_s g_v |\mu|}{4\pi\hbar^2} \frac{i}{\omega + i\gamma} = \frac{n_s e^2 V^2}{|\mu|} \frac{i}{\omega + i\gamma} = \frac{n_s e^2}{m^\star} \frac{i}{\omega + i\gamma}, \tag{27}$$

where the last equalities are written in the Drude form with the phenomenological scattering rate $\gamma$, the "effective mass" of graphene quasiparticles at the Fermi level $m^\star = |\mu|/V^2$ and the charge carrier density

$$n_s = \frac{g_s g_v}{4} \frac{\mu^2}{\pi\hbar^2 V^2} = \frac{g_s g_v}{4} \frac{k_F^2}{\pi}. \tag{28}$$

The value $k_F$ in (28) is the Fermi wavevector.

The intra-band conductivity has a standard Drude form. In the collisionless approximation $\omega \gg \gamma$ it is an imaginary function which falls down with the growing frequency as $1/\omega$. In the currently available graphene samples with the mobility $\mu_e \simeq 200000$ cm$^2$/Vs Orlita et al. (2008); Geim (2009) and the electron density $n_s \simeq 10^{12}$ cm$^{-2}$ the condition $\omega \gtrsim \gamma$ is satisfied at $\omega/2\pi \gtrsim 0.1$ THz.

### 3.3 Inter-band conductivity

For the inter-band conductivity $\sigma^{inter}_{\alpha\beta}(\omega)$ which is dominant at high (infrared, optical) frequencies we get in the limit $\mathbf{q} \to \mathbf{0}$

$$\sigma^{inter}_{\alpha\beta}(\omega) = \frac{ie^2\hbar g_s}{S} \sum_{\mathbf{k}, l\neq l'} \frac{f(E_{l'\mathbf{k}}) - f(E_{l\mathbf{k}})}{E_{l'\mathbf{k}} - E_{l\mathbf{k}} - \hbar(\omega + i\gamma)} \frac{\langle l\mathbf{k}|\hat{v}_\alpha|l'\mathbf{k}\rangle\langle l'\mathbf{k}|\hat{v}_\beta|l\mathbf{k}\rangle}{E_{l'\mathbf{k}} - E_{l\mathbf{k}}}. \tag{29}$$

Using the matrix elements (15), assuming that $\gamma \to 0$ and considering again only the vicinity of Dirac points one gets $\sigma^{inter}_{\alpha\beta}(\omega) = \sigma^{inter}(\omega)\delta_{\alpha\beta}$, where

$$\sigma^{inter}(\omega) = \frac{ie^2 g_s g_v}{16\pi\hbar} \int_0^\infty dk \frac{\sinh(\hbar V k/T)}{\cosh(\mu/T) + \cosh(\hbar V k/T)} \left(\frac{1}{k + \omega/2V + i0} - \frac{1}{k - \omega/2V - i0}\right). \tag{30}$$

The real part of the inter-band conductivity (30) is calculated analytically at all values of $\omega$, $\mu$ and $T$,

$$\mathrm{Re}\,\sigma^{inter}(\omega) = \frac{e^2 g_s g_v}{16\hbar} \frac{\sinh(\hbar|\omega|/2T)}{\cosh(\mu/T) + \cosh(\hbar|\omega|/2T)}. \tag{31}$$

At high frequencies $\hbar\omega \gg |\mu|, T$ this gives the remarkable result of the universal optical conductivity

$$\sigma^{opt}(\omega) = \frac{e^2 g_s g_v}{16\hbar} = \frac{e^2}{4\hbar}, \quad \hbar\omega \gg |\mu|, T, \tag{32}$$

which depends only on the fundamental constants $e$ and $\hbar$, Ando et al. (2002); Kuzmenko et al. (2008); Nair et al. (2008). The imaginary part is determined by the principal value integral

$$\mathrm{Im}\,\sigma^{inter}(\omega) = \frac{e^2 g_s g_v}{16\pi\hbar}\int_0^\infty dx \frac{\sinh x}{\cosh(|\mu|/T)+\cosh x}\left(\frac{1}{x+\hbar\omega/2T}-\frac{1}{x-\hbar\omega/2T}\right), \quad (33)$$

which can be analytically calculated at low temperatures $T \ll |\mu|$. Together with the real part this gives

$$\sigma^{inter}(\omega) = \frac{e^2 g_s g_v}{16\hbar}\left(\theta(\hbar\omega-2\mu)+\frac{i}{\pi}\ln\left|\frac{1-\hbar\omega/2|\mu|}{1+\hbar\omega/2|\mu|}\right|\right), \quad (34)$$

see Figure 4. At high frequencies the inter-band conductivity tends to a (universal) constant and exceeds the intra-band contribution if $\hbar\omega \gtrsim |\mu|$. Finally, the total conductivity $\sigma(\omega) = \sigma^{intra}(\omega)+\sigma^{inter}(\omega)$ in the collisionless limit $\omega \gg \gamma$ has the form

$$\sigma(\omega) = \frac{e^2 g_s g_v}{16\hbar}\left(\frac{4i|\mu|}{\pi\hbar\omega}+\theta(\hbar\omega-2|\mu|)+\frac{i}{\pi}\ln\left|\frac{1-\hbar\omega/2|\mu|}{1+\hbar\omega/2|\mu|}\right|\right) \quad (35)$$

and is shown in Figure 5.

Summarizing the linear response results on the dynamic conductivity of graphene one sees that at low frequencies $\hbar\omega \ll |\mu|$ the conductivity $\sigma(\omega)$ is imaginary and is described by the classical Drude formula. It corresponds to the intra-band response of the system. At high frequencies $\hbar\omega \gg |\mu|$ the real part of the quantum inter-band conductivity dominates. At the typical charge carrier densities of $n_s \simeq 10^{11}-10^{13}$ cm$^{-2}$ the transition between the two regimes $\hbar\omega \simeq |\mu|$ lies in graphene at the frequencies $\omega/2\pi \simeq 10-100$ THz. The low-frequency limit $\hbar\omega \ll |\mu|$ thus corresponds to the radio, microwave and terahertz frequencies, while the high-frequency limit – to the infrared and optical frequencies. The collisions can be ignored, in the high quality samples, at $\omega/2\pi \gtrsim 0.1$ THz.

## 4. Frequency mixing: Quasi-classical theory

In this Section we consider the frequency mixing effect using the quasi-classical approach based on the solution of the kinetic Boltzmann equation. The quasi-classical solution is simpler and, within the collisionless approximation, can be obtained non-perturbatively, at arbitrary values of the external electric field amplitudes Mikhailov (2007). The quasi-classical theory is valid at $\hbar\omega \ll |\mu|$, which corresponds to the very broad and technologically important range of radio, microwave and terahertz frequencies.

### 4.1 Boltzmann kinetic equation

Consider the classical motion of massless particles (1) under the action of the external electric field $\mathbf{E}(t)$. The evolution of the electron distribution function $f_{\mathbf{p}}(t)$ is determined by the Boltzmann kinetic equation which has the form

$$\frac{\partial f_{\mathbf{p}}}{\partial t} - e\mathbf{E}(t)\frac{\partial f_{\mathbf{p}}}{\partial \mathbf{p}} = 0 \quad (36)$$

in the collisionless approximation. Its exact solution is

$$f(\mathbf{p},t) = \left[1+\exp\left(\frac{V|\mathbf{p}-\mathbf{p}_0(t)|-\mu}{T}\right)\right]^{-1}, \quad (37)$$

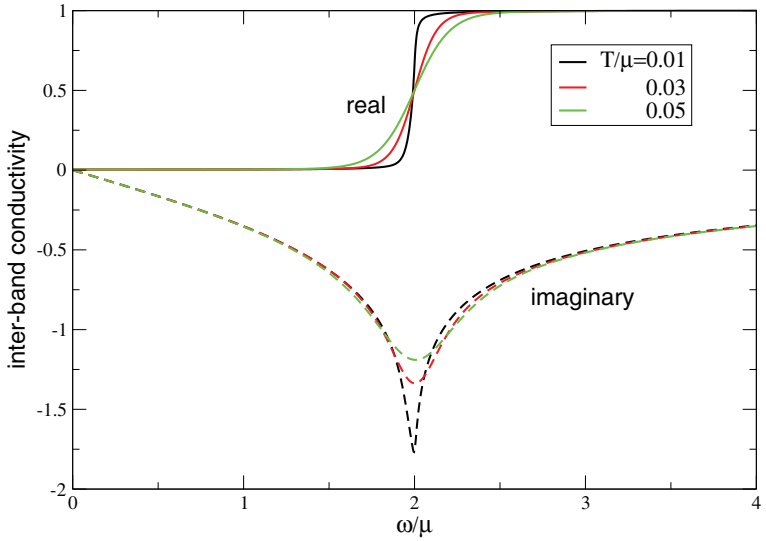


Fig. 4. The inter-band conductivity of graphene at $\gamma/\mu = 0.01$ and three different temperatures as shown in the Figure. The conductivity is measured in units $e^2 g_s g_s/16\hbar$.

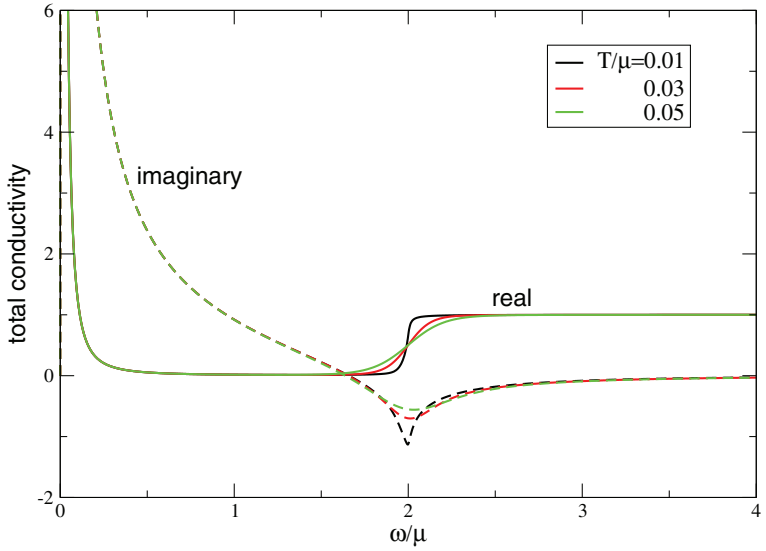


Fig. 5. The total conductivity of graphene at $\gamma/\mu = 0.01$ and three different temperatures as shown in the Figure. The conductivity is measured in units $e^2 g_s g_s/16\hbar$. At low frequencies $\hbar\omega \lesssim |\mu|$ the conductivity is imaginary and corresponds to the intra-band classical contribution. At high frequencies $\hbar\omega \gtrsim |\mu|$ the quantum inter-band contribution dominates.

where $\mathbf{p}_0(t)$ satisfies the classical equation of motion $d\mathbf{p}_0(t)/dt = -e\mathbf{E}(t)$. The current can then be calculated as

$$\mathbf{j}(t) = -e\frac{g_s g_v V}{(2\pi\hbar)^2}\int dp_x dp_y \frac{\mathbf{p}}{\sqrt{p_x^2+p_y^2}}\frac{1}{1+\exp\left(\frac{V|\mathbf{p}-\mathbf{p}_0(t)|-\mu}{T}\right)}. \tag{38}$$

Assuming now that the temperature is low, $T \ll \mu$, and expanding the right-hand side of Eq. (38) we get

$$-\frac{\mathbf{j}(t)}{en_sV} = \frac{\mathbf{P}(t)}{\sqrt{P^2(t)+1}}\left[1+\frac{3}{8}\frac{P^2(t)}{[P^2(t)+1]^2}\right], \tag{39}$$

where

$$\mathbf{P}(t) = \frac{\mathbf{p}_0(t)}{p_F}. \tag{40}$$

Notice that the expansion parameter in Eq. (39) is $|P(t)/(P^2(t)+1)| \ll 1$, i.e. the result (39) is valid both at small and large $|P(t)|$. In the regime of low electric fields $|P(t)| \ll 1$ the current is

$$-\frac{\mathbf{j}(t)}{en_sV} \approx \mathbf{P}(t)\left(1-\frac{1}{8}P^2(t)\right). \tag{41}$$

### 4.2 Frequency mixing response

If the graphene layer is irradiated by two waves with the frequencies $\omega_1$, $\omega_2$ and the both waves are linearly polarized in the same direction,

$$\mathbf{E}(t) = \mathbf{E}_1\cos\omega_1 t + \mathbf{E}_2\cos\omega_2 t, \;\; \mathbf{E}_1 \parallel \mathbf{E}_2, \tag{42}$$

then

$$\mathbf{p}_0(t) = -e\left(\frac{\mathbf{E}_1}{\omega_1}\sin\omega_1 t + \frac{\mathbf{E}_2}{\omega_2}\sin\omega_2 t\right), \tag{43}$$

the current is parallel to the electric fields and equals

$$\begin{aligned}\frac{j(t)}{en_sV} &= \alpha_1\left(1-\frac{3}{32}\alpha_1^2-\frac{3}{16}\alpha_2^2\right)\sin\omega_1 t \\ &+ \frac{\alpha_1^3}{32}\sin 3\omega_1 t + \frac{3\alpha_1^2\alpha_2}{32}\Big[\sin(2\omega_1+\omega_2)t - \sin(2\omega_1-\omega_2)t\Big] + \ldots,\end{aligned} \tag{44}$$

where

$$\alpha_j = \frac{eE_j}{p_F\omega_j} = \frac{eE_jV}{|\mu|\omega_j}, \;\; j=1,2. \tag{45}$$

The omitted terms marked by the dots are obtained from the present ones by replacing $\omega_1 \leftrightarrow \omega_2$ and $\alpha_1 \leftrightarrow \alpha_2$. We will call $\alpha_j$ the *field parameters*. The field parameter $\alpha = eEV/\mu\omega$ is the work done by the electric field during one oscillation period ($eEV/\omega$) divided by the average energy of electrons $\mu$, Mikhailov (2007).

If the field parameters are small, $\alpha_j \ll 1$, Eq. (44) describes the low-frequency linear response, since $en_sV\alpha_j = \sigma^{intra}(\omega_j)E_j$, see Eq. (27). If $\alpha_j$ are not negligible, the first line in (44) represents the second order corrections to the linear conductivity, the first term in the second line gives the third harmonics generation effect, Mikhailov (2007), and the last terms in the second line – the frequency mixing. The amplitudes of the third-order mixed frequency current $j^{(3)}_{(2\omega_1\pm\omega_2)}(t) = j^{(3)}_{(2\omega_1\pm\omega_2)}\sin(\omega_2 \pm 2\omega_1)t$ can be rewritten as

$$j^{(3)}_{(2\omega_1\pm\omega_2)} = \frac{3}{32}en_sV\left(\frac{eE_1}{p_F\omega_1}\right)^2\frac{eE_2}{p_F\omega_2} = \frac{3}{32}\sigma^{intra}(\omega_2)E_2\alpha_1^2, \tag{46}$$

i.e., up to a numerical factor, the third order current is the product of the low-frequency Drude conductivity (27), the electric field $E_2$ and the squared field parameter $\alpha_1^2$. One sees that the amplitude of the third order mixed-frequency current will be comparable with the linear response current if the field parameter $\alpha$ is of order unity (or larger). This means that the required electric field is determined by the inequality

$$E \gtrsim \frac{p_F \omega}{e} = \frac{\hbar\omega\sqrt{\pi n_s}}{e}. \tag{47}$$

The lower the charge carrier density $n_s$ and the radiation frequency $\omega$ the smaller is the electric field needed for the observation of the nonlinear effects. If, for example, the density is $\simeq 10^{11}$ cm$^{-2}$ and the frequency is $\simeq 0.5$ THz, Eq. (47) gives $E \gtrsim 1$ kV/cm which corresponds to the incident wave power $\simeq 2$ kW/cm$^2$.
If the linear polarizations of the two incident waves $\omega_1$ and $\omega_2$ are perpendicular to each other, $\mathbf{E}_1 \cdot \mathbf{E}_2 = 0$, the current at the mixed frequencies $2\omega_1 \pm \omega_2$ is three times smaller than for the parallel polarization. This is a general result which is also valid in the quantum regime.

## 5. Frequency mixing: Quantum theory

The full quantum theory of the nonlinear frequency mixing effects in graphene is substantially more complicated and is yet to be developed. In this paper we only consider the frequency mixing response at the frequency $\omega_e \equiv 2\omega_1 - \omega_2$ and calculate it under the conditions

$$\hbar\omega_1,\ \hbar\omega_2,\ \hbar\omega_e \gg |\mu|, \tag{48}$$

relevant for the experiment of Hendry et al. (2010).

### 5.1 Quantum kinetic (Liouville) equation

In order to investigate the nonlinear response problem in the quantum regime (48) we have to solve the quantum kinetic equation (16) in, at least, the third order in the external field amplitudes $E_j$, $j = 1, 2$. We do this using the perturbation theory. Expanding the density matrix $\hat{\rho}$ in powers of the electric fields, $\hat{\rho} = \hat{\rho}_0 + \hat{\rho}_1 + \hat{\rho}_2 + \hat{\rho}_3 + \ldots$, we get from (16) a set of recurrent equations

$$i\hbar\frac{\partial\hat{\rho}_n}{\partial t} = [\hat{H}_0, \hat{\rho}_n] + [\hat{H}_1, \hat{\rho}_{n-1}],\ \ n = 2, 3, \ldots \tag{49}$$

for $\hat{\rho}_n$. At high frequencies (48) we can write the Hamiltonian $\hat{H}_1$ in the form

$$\hat{H}_1 = (eE_1 x\cos\omega_1 t + eE_2 x\cos\omega_2 t)\, e^{\gamma t} = h_{\omega_1} e^{i(\omega_1 - i0)t} + h_{\omega_2} e^{i(\omega_2 - i0)t} + \{\omega_j \to -\omega_j\}, \tag{50}$$

where $h_{\omega_1} = h_{-\omega_1} = eE_1 x/2$, $h_{\omega_2} = h_{-\omega_2} = eE_2 x/2$ and it is assumed that $\gamma \to 0$. In the first order in $E_j$ we get

$$\langle\lambda|\hat{\rho}_1|\lambda'\rangle = \sum_{\omega=\{\pm\omega_1,\pm\omega_2\}} \frac{f_{\lambda'} - f_\lambda}{E_{\lambda'} - E_\lambda - \hbar\omega + i0}\langle\lambda|h_\omega|\lambda'\rangle e^{i\omega t} \equiv \sum_{\omega\{\pm\omega_1,\pm\omega_2\}} \rho_{1\omega} e^{i\omega t}, \tag{51}$$

where we have used a short notation $|\lambda\rangle$ for the set of three quantum numbers $|l\mathbf{k}\sigma\rangle$. The right hand side of Eq. (51) contains the oscillating exponents with the frequencies $\pm\omega_1$ and $\pm\omega_2$. For the matrix elements of $\hat{\rho}_2$ we obtain, similarly,

$$\langle\lambda|\hat{\rho}_2|\lambda'\rangle = \sum_{\omega_a,\omega_b} \frac{\langle\lambda|[h_{\omega_a}, \rho_{1\omega_b}]|\lambda'\rangle}{E_{\lambda'} - E_\lambda - \hbar\omega_a - \hbar\omega_b + i0} e^{i(\omega_a+\omega_b)t}. \tag{52}$$

The summation here is performed over the sets of frequencies $\omega_a = \{\pm\omega_1, \pm\omega_2\}$ and $\omega_b = \{\pm\omega_1, \pm\omega_2\}$, i.e. the right hand side in (52) contains the oscillating terms with the frequencies $\pm 2\omega_1$, $\pm 2\omega_2$, $\pm(\omega_1+\omega_2)$, $\pm(\omega_1-\omega_2)$ and a time independent term with $\omega = 0$. We will denote this set of frequencies as $\omega_c = \{\pm 2\omega_1, \pm 2\omega_2, \pm(\omega_1+\omega_2), \pm(\omega_1-\omega_2), 0\}$. The commutator $[h_{\omega_a}, \rho_{1\omega_b}]$ is calculated as

$$\langle\lambda|[h_{\omega_a}, \rho_{1\omega_b}]|\lambda'\rangle = \sum_{\lambda''}\Big(\langle\lambda|h_{\omega_a}|\lambda''\rangle\langle\lambda''|\rho_{1\omega_b}|\lambda'\rangle - \langle\lambda|\rho_{1\omega_b}|\lambda''\rangle\langle\lambda''|h_{\omega_a}|\lambda'\rangle\Big),$$

where the matrix elements $\langle\lambda|h_\omega|\lambda'\rangle$ and $\langle\lambda|\rho_{1\omega}|\lambda'\rangle$ are known from (14) and (51).
Then, for the matrix elements of $\hat{\rho}_3$ we get

$$\langle\lambda|\hat{\rho}_3|\lambda'\rangle = \sum_{\omega_a,\omega_c}\frac{\langle\lambda|[h_{\omega_a}, \rho_{2\omega_c}]|\lambda'\rangle}{E_{\lambda'} - E_\lambda - \hbar\omega_a - \hbar\omega_c + i0}e^{i(\omega_a+\omega_c)t}. \tag{53}$$

Now the right hand side of Eq. (53) contains the terms with the frequencies $\pm\omega_1$, $\pm\omega_2$, $\pm 3\omega_1$, $\pm 3\omega_2$, $\pm(2\omega_1 \pm \omega_2)$ and $\pm(2\omega_2 \pm \omega_1)$.
The general formulas (51), (52) and (53) allows one, in principle, to calculate the time dependence of the matrix elements of the density matrix in the third order in $E_j$. Then, using the formula

$$j_\alpha(t) = -\frac{e}{S}\sum_{\lambda\lambda'}\langle\lambda'|\hat{v}_\alpha|\lambda\rangle\langle\lambda|\hat{\rho}_1 + \hat{\rho}_2 + \hat{\rho}_3 + \ldots|\lambda'\rangle \tag{54}$$

one can find the time dependence of the current in the same order of the perturbation theory. This general expression for the current will contain the terms with the frequencies $\omega_1$, $\omega_2$, $3\omega_1$, $3\omega_2$, as well as $(2\omega_1 \pm \omega_2)$ and $(2\omega_2 \pm \omega_1)$.

### 5.2 Optical frequency mixing at $\omega_e = 2\omega_1 - \omega_2$

Being interested in this work only in the response at the frequency of the emitted light $\omega_e \equiv 2\omega_1 - \omega_2$ (see Hendry et al. (2010)) we get, after quite lengthy calculations,

$$\begin{aligned} j^{(3)}_{(\omega_e)}(t) = {} & \frac{e^4 g_s}{8\hbar^2}E_1^2E_2\frac{2\omega_1-\omega_2}{\omega_1(\omega_1-\omega_2)^2}e^{i\omega_e t}\frac{1}{S}\sum_{\mathbf{k}}(f_{2\mathbf{k}} - f_{1\mathbf{k}})\langle 1\mathbf{k}|v_x|2\mathbf{k}\rangle\langle 1\mathbf{k}|x|2\mathbf{k}\rangle^3 \\ & \times\left(-\frac{2}{E_{2\mathbf{k}} - E_{1\mathbf{k}} + \hbar\omega_1 - i0} + \frac{2}{E_{2\mathbf{k}} - E_{1\mathbf{k}} - \hbar\omega_1 + i0}\right. \\ & + \frac{1}{E_{2\mathbf{k}} - E_{1\mathbf{k}} + \hbar\omega_2 - i0} - \frac{1}{E_{2\mathbf{k}} - E_{1\mathbf{k}} - \hbar\omega_2 + i0} \\ & \left. - \frac{1}{E_{2\mathbf{k}} - E_{1\mathbf{k}} - \hbar\omega_e + i0} + \frac{1}{E_{2\mathbf{k}} - E_{1\mathbf{k}} + \hbar\omega_e - i0}\right) + (\omega_j \to -\omega_j). \end{aligned} \tag{55}$$

The current $j^{(3)}_{(\omega_e)}(t)$ contains the resonant terms corresponding to the vertical optical transitions at $E_{2\mathbf{k}} - E_{1\mathbf{k}} = \hbar\omega_1$, $\hbar\omega_2$ and $\hbar\omega_e$. As it follows from the linear response theory (Section 3), the largest contribution to the current at the optical frequencies $\hbar\omega \gg |\mu|$ is given by the absorption terms proportional to $\delta(E_{2\mathbf{k}} - E_{1\mathbf{k}} - \hbar\omega)$. The same is valid in the nonlinear

regime too. Taking into account in (55) only the terms $\propto \delta(E_{2\mathbf{k}} - E_{1\mathbf{k}} - \hbar\omega_{1,2,e})$ we finally get

$$j^{(3)}_{(\omega_e)}(t) \approx \frac{3e^4 g_s g_v V^2}{256\hbar^3} E_1^2 E_2 \frac{2\omega_1 - \omega_2}{\omega_1(\omega_1 - \omega_2)^2}\left[\frac{2}{\omega_1^2} - \frac{1}{\omega_2^2} - \frac{1}{(2\omega_1 - \omega_2)^2}\right]\cos(2\omega_1 - \omega_2)t$$
$$= -\frac{9}{8}\sigma^{opt}(\omega_2)E_2\beta_1^2 F\left(\frac{\omega_2}{\omega_1}\right)\cos(2\omega_1 - \omega_2)t, \tag{56}$$

where

$$\beta_1 = \frac{eE_1 V}{\hbar\omega_1^2} \tag{57}$$

is the *optical* field parameter and

$$F(x) = \frac{2 + 2x - x^2}{3x^2(2 - x)}. \tag{58}$$

Eq. (56) is the main result of this work. It represents the ac electric current induced in the graphene layer at the frequency $\omega_e = 2\omega_1 - \omega_2$ by the two incident waves (42) polarized in the same direction (the current direction coincides with that of the fields). If the two incident waves are perpendicularly polarized, the numerical prefactor in (56) is reduced ($9/8 \to 3/8$). As seen from (56), at high frequencies the current depends neither on the chemical potential $\mu$ nor on the temperature $T$ as it should be under the conditions when the vertical inter-band transitions play the main role. The second line of (56) is written in the form similar to (46): at the optical frequencies the current is the product of the high-frequency, universal optical conductivity (32), the electric field $E_2$ and the squared field parameter $\beta_1^2$. The *optical* field parameter $\beta = eEV/\hbar\omega^2$ is the work done by the electric field during one oscillation period ($eEV/\omega$) divided by the photon energy $\hbar\omega$ (instead of the Fermi energy $\mu$ at low frequencies, Eq. (45)). In addition to the mentioned parameters, the current (56) weakly depends on the ratio of the two optical frequencies $\omega_2/\omega_1$ which is described by the function (58) shown in Figure 6. The function $F(x)$ is of order unity if the difference $\omega_2 - \omega_1$ is not very large. If $\omega_1$, $\omega_2$ or $\omega_e$ tend to zero the current (56) has a strong tendency to grow. These limits are very interesting for future studies but have been excluded from the current consideration by the conditions (48).

The formula (56) is in good quantitative agreement with the experimental results of Hendry et al. (2010). The comparison with other materials made in that paper showed that graphene has much stronger nonlinear properties than typical nonlinear insulators and some metals (Au). Comparing the experimental results of Hendry et al. (2010) with those of Erokhin et al. (1987) shows that graphene is also a stronger nonlinear material than a typical nonlinear semiconductor InSb. Further theoretical and experimental studies of the nonlinear electrodynamic and optical properties of graphene are therefore highly desirable.

## 6. Summary and conclusions

Due to the massless energy spectrum of the charge carriers graphene demonstrates strongly nonlinear electromagnetic properties. In this work we have developed a theory of the nonlinear frequency mixing effect in graphene. The two physically different regimes have been considered. At low frequencies, corresponding to the radio, microwave and terahertz range, the problem is solved within the quasi-classical approach which takes into account the intra-band response of the material. At high frequencies, corresponding to the infrared and

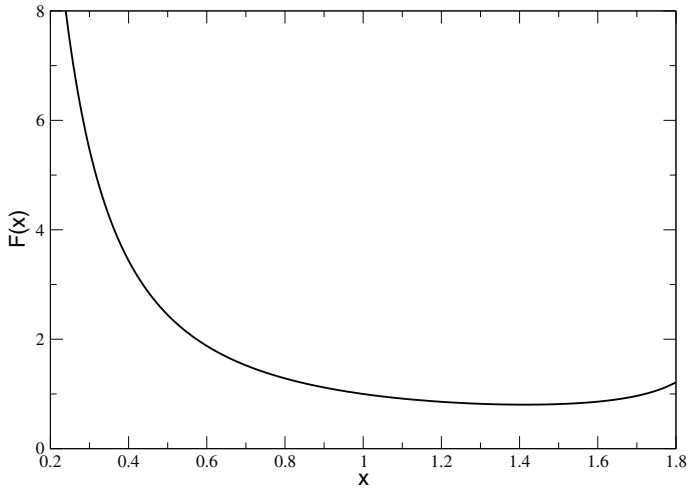


Fig. 6. The function $F(x)$ from Eq. (58).

visible light, a quantum theory is developed which takes into account the inter-band optical transitions.

At the optical frequencies our results quantitatively agree with the recent experimental findings of Hendry et al. (2010) who have observed the nonlinear electromagnetic response of graphene for the first time. The results of Hendry et al. (2010) show that in the visible and near-infrared frequency range the nonlinear parameters of graphene are much stronger than in many other nonlinear materials. Even more important conclusion is that, according to our theoretical predictions, the nonlinear response of graphene substantially grows at lower frequencies. One should expect therefore even stronger nonlinear properties of graphene at the mid-infrared, terahertz and microwave frequencies which would be of extreme importance for the future progress of the nonlinear terahertz- and optoelectronics.

The author thanks the Deutsche Forschungsgemeinschaft for support of this work.

## 7. References

Abergel, D. S. L. & Fal'ko, V. I. (2007). Optical and magneto-optical far-infrared properties of bilayer graphene, *Phys. Rev. B* 75: 155430.

Ando, T., Zheng, Y. & Suzuura, H. (2002). Dynamical conductivity and zero-mode anomaly in honeycomb lattices, *J. Phys. Soc. Japan* 71: 1318–1324.

Castro Neto, A. H., Guinea, F., Peres, N. M. R., Novoselov, K. S. & Geim, A. K. (2009). The electronic properties of graphene, *Rev. Mod. Phys.* 81: 109–162.

Dawlaty, J. M., Shivaraman, S., Strait, J., George, P., Chandrashekhar, M., Rana, F., Spencer, M. G., Veksler, D. & Chen, Y. (2008). Measurement of the optical absorption spectra of epitaxial graphene from terahertz to visible, *Appl. Phys. Lett.* 93: 131905.

Erokhin, A. I., Kovalev, V. I. & Shmelev, A. K. (1987). Nonlinear susceptibility of InSb at the wavelength of 10.6 $\mu$m, *Sov. J. Quantum Electron.* 17: 742–745.

Falkovsky, L. A. & Pershoguba, S. S. (2007). Optical far-infrared properties of a graphene monolayer and multilayer, *Phys. Rev. B* 76: 153410.

Falkovsky, L. A. & Varlamov, A. A. (2007). Space-time dispersion of graphene conductivity, *Europ. Phys. J. B* 56: 281–284.
Geim, A. K. (2009). Graphene: Status and prospects, *Science* 324: 1530–1534.
Gusynin, V. P. & Sharapov, S. G. (2006). Transport of Dirac quasiparticles in graphene: Hall and optical conductivities, *Phys. Rev. B* 73: 245411.
Gusynin, V. P., Sharapov, S. G. & Carbotte, J. P. (2006). Unusual microwave response of Dirac quasiparticles in graphene, *Phys. Rev. Lett.* 96: 256802.
Hendry, E., Hale, P. J., Moger, J., Savchenko, A. K. & Mikhailov, S. A. (2010). Coherent nonlinear optical response of graphene, *Phys. Rev. Lett.* 105: 097401.
Katsnelson, M. I. (2006). Minimal conductivity in bilayer graphene, *Europ. Phys. J. B* 52: 151–153.
Katsnelson, M. I. (2007). Graphene: carbon in two dimensions, *Materials Today* 10: 20–27.
Kuzmenko, A. B., van Heumen, E., Carbone, F. & van der Marel, D. (2008). Universal optical conductance of graphite, *Phys. Rev. Lett.* 100: 117401.
Li, Z. Q., Henriksen, E. A., Jiang, Z., Hao, Z., Martin, M. C., Kim, P., Stormer, H. L. & Basov, D. N. (2008). Dirac charge dynamics in graphene by infrared spectroscopy, *Nature Physics* 4: 532–535.
López-Rodríguez, F. J. & Naumis, G. G. (2008). Analytic solution for electrons and holes in graphene under electromagnetic waves: Gap appearance and nonlinear effects, *Phys. Rev. B* 78: 201406(R).
Mak, K. F., Sfeir, M. Y., Wu, Y., Lui, C. H., Misewich, J. A. & Heinz, T. F. (2008). Measurement of the optical conductivity of graphene, *Phys. Rev. Lett.* 101: 196405.
McClure, J. W. (1956). Diamagnetism of graphite, *Phys. Rev.* 104: 666–671.
Mikhailov, S. A. (2007). Non-linear electromagnetic response of graphene, *Europhys. Lett.* 79: 27002.
Mikhailov, S. A. (2008). Electromagnetic response of electrons in graphene: Non-linear effects, *Physica E* 40: 2626–2629.
Mikhailov, S. A. (2009). Non-linear graphene optics for terahertz applications, *Microelectron. J.* 40: 712–715.
Mikhailov, S. A. & Ziegler, K. (2007). New electromagnetic mode in graphene, *Phys. Rev. Lett.* 99: 016803.
Mikhailov, S. A. & Ziegler, K. (2008). Non-linear electromagnetic response of graphene: Frequency multiplication and the self-consistent field effects, *J. Phys. Condens. Matter* 20: 384204.
Nair, R. R., Blake, P., Grigorenko, A. N., Novoselov, K. S., Booth, T. J., Stauber, T., Peres, N. M. R. & Geim, A. K. (2008). Fine structure constant defines visual transparency of graphene, *Science* 320: 1308–1308.
Nilsson, J., Castro Neto, A. H., Guinea, F. & Peres, N. M. R. (2006). Electronic properties of graphene multilayers, *Phys. Rev. Lett.* 97: 266801.
Nomura, K. & MacDonald, A. H. (2007). Quantum transport of massless Dirac fermions, *Phys. Rev. Lett.* 98: 076602.
Novoselov, K. S., Geim, A. K., Morozov, S. V., Jiang, D., Katsnelson, M. I., Grigorieva, I. V., Dubonos, S. V. & Firsov, A. A. (2005). Two-dimensional gas of massless Dirac fermions in graphene, *Nature* 438: 197–200.
Novoselov, K. S., Geim, A. K., Morozov, S. V., Jiang, D., Zhang, Y., Dubonos, S. V., Grigorieva, I. V. & Firsov, A. A. (2004). Electric field effect in atomically thin carbon films, *Science* 306: 666–669.

Novoselov, K. S., Jiang, Z., Zhang, Y., Morozov, S. V., Stormer, H. L., Zeitler, U., Maan, J. C., Boebinger, G. S., Kim, P. & Geim, A. K. (2007). Room-temperature quantum Hall effect in graphene, *Science* 315: 1379.

Orlita, M., Faugeras, C., Plochocka, P., Neugebauer, P., Martinez, G., Maude, D. K., Barra, A.-L., Sprinkle, M., Berger, C., de Heer, W. A. & Potemski, M. (2008). Approaching the Dirac point in high-mobility multilayer epitaxial graphene, *Phys. Rev. Lett.* 101: 267601.

Peres, N. M. R., Stauber, T. & Castro Neto, A. H. (2008). The infrared conductivity of graphene, *Europhys. Lett.* 84: 38002.

Reich, S., Maultzsch, J., Thomsen, C. & Ordejon, P. (2002). Tight-binding description of graphene, *Phys. Rev. B* 66: 035412.

Slonczewski, J. C. & Weiss, P. R. (1958). Band structure of graphite, *Phys. Rev.* 109(2): 272–279.

Stander, N., Huard, B. & Goldhaber-Gordon, D. (2009). Evidence for Klein tunneling in graphene *p-n* junctions, *Phys. Rev. Lett.* 102: 026807.

Stauber, T., Peres, N. M. R. & Castro Neto, A. H. (2008). Conductivity of suspended and non-suspended graphene at finite gate voltage, *Phys. Rev. B* 78: 085418.

Stauber, T., Peres, N. M. R. & Geim, A. K. (2008). Optical conductivity of graphene in the visible region of the spectrum, *Phys. Rev. B* 78: 085432.

Tan, Y.-W., Zhang, Y., Bolotin, K., Zhao, Y., Adam, S., Hwang, E. H., Das Sarma, S., Stormer, H. L. & Kim, P. (2007). Measurement of scattering rate and minimum conductivity in graphene, *Phys. Rev. Lett.* 99: 246803.

Wallace, P. R. (1947). The band theory of graphite, *Phys. Rev.* 71(9): 622–634.

Young, A. F. & Kim, P. (2009). Quantum interference and Klein tunnelling in graphene heterojunctions, *Nature Physics* 5: 222–226.

Zhang, Y., Tan, Y.-W., Stormer, H. L. & Kim, P. (2005). Experimental observation of the quantum Hall effect and Berry's phase in graphene, *Nature* 438: 201–204.

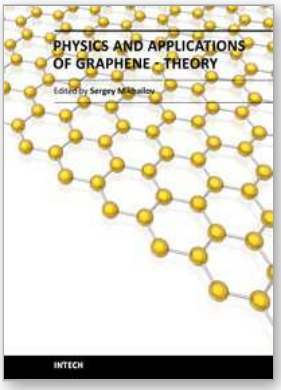


**Physics and Applications of Graphene - Theory**

Edited by Dr. Sergey Mikhailov

ISBN 978-953-307-152-7
Hard cover, 534 pages
**Publisher** InTech
**Published online** 22, March, 2011
**Published in print edition** March, 2011

The Stone Age, the Bronze Age, the Iron Age... Every global epoch in the history of the mankind is characterized by materials used in it. In 2004 a new era in material science was opened: the era of graphene or, more generally, of two-dimensional materials. Graphene is the strongest and the most stretchable known material, it has the record thermal conductivity and the very high mobility of charge carriers. It demonstrates many interesting fundamental physical effects and promises a lot of applications, among which are conductive ink, terahertz transistors, ultrafast photodetectors and bendable touch screens. In 2010 Andre Geim and Konstantin Novoselov were awarded the Nobel Prize in Physics "for groundbreaking experiments regarding the two-dimensional material graphene". The two volumes Physics and Applications of Graphene - Experiments and Physics and Applications of Graphene - Theory contain a collection of research articles reporting on different aspects of experimental and theoretical studies of this new material.



INTECH
open science | open minds

**InTech Europe**
University Campus STeP Ri
Slavka Krautzeka 83/A
51000 Rijeka, Croatia
Phone: +385 (51) 770 447
Fax: +385 (51) 686 166
www.intechopen.com

**InTech China**
Unit 405, Office Block, Hotel Equatorial Shanghai
No.65, Yan An Road (West), Shanghai, 200040, China
中国上海市延安西路65号上海国际贵都大饭店办公楼405单元
Phone: +86-21-62489820
Fax: +86-21-62489821